JACS
JOURNAL OF THE AMERICAN CHEMICAL SOCIETY
Article
pubs.acs.org/JACS

Nanocrystal Diffusion Doping

Vladimir A. Vlaskin, Charles J. Barrows, Christian S. Erickson, and Daniel R. Gamelin*

Department of Chemistry, University of Washington, Seattle, Washington 98195-1700, United States

Supporting Information

ABSTRACT: A diffusion-based synthesis of doped colloidal semiconductor nanocrystals is demonstrated. This approach involves thermodynamically controlled addition of both impurity cations and host anions to preformed seed nanocrystals under equilibrium conditions, rather than kinetically controlled doping during growth. This chemistry allows thermodynamic crystal compositions to be prepared without sacrificing other kinetically trapped properties such as shape, size, or crystallographic phase. This doping chemistry thus shares some similarities with cation-exchange reactions, but proceeds without the loss of host cations and excels at the introduction of relatively unreactive impurity ions that have not been previously accessible using cation exchange. Specifically, we demonstrate the preparation of $Cd_{1-x}Mn_xSe$ ($0 \leq x \leq \sim 0.2$) nanocrystals with narrow size distribution, unprecedentedly high Mn^{2+} content, and very large magneto-optical effects by diffusion of Mn^{2+} into seed CdSe nanocrystals grown by hot injection. Controlling the solution and lattice chemical potentials of Cd^{2+} and Mn^{2+} allows Mn^{2+} diffusion into the internal volumes of the CdSe nanocrystals with negligible Ostwald ripening, while retaining the crystallographic phase (wurtzite or zinc blende), shape anisotropy, and ensemble size uniformity of the seed nanocrystals. Experimental results for diffusion doping of other nanocrystals with other cations are also presented that indicate this method may be generalized, providing access to a variety of new doped semiconductor nanostructures not previously attainable by kinetic routes or cation exchange.

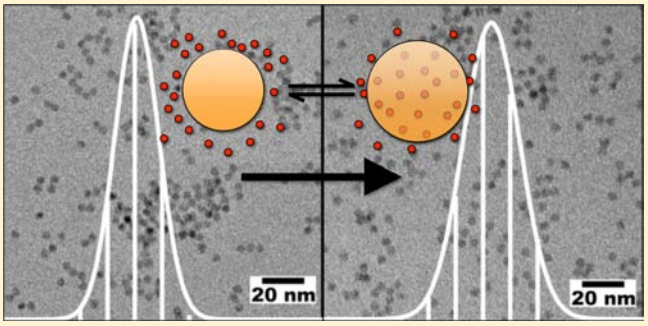

INTRODUCTION

The physical properties of inorganic crystals can be changed dramatically by the introduction of impurities. The development of synthetic methods for growing high-quality doped inorganic crystals has consequently been a perennial frontier of materials science, laying the foundation for such technological milestones as the ruby laser and silicon microelectronics. The past two decades have seen the emergence of another frontier in crystal growth that exploits the ability to isolate kinetically trapped semiconductor nanocrystals, often with anisotropic shapes, before they evolve into their macroscopic thermodynamic end products. Colloidal CdSe nanocrystals have played a central role in the advancement of this field,[1−5] serving as a model system for the development of optimized syntheses controlling structural quality, nanocrystal uniformity, and shape anisotropies, and ultimately translating these features into powerful physical properties.[6,7] For almost as long, however, it has also been recognized that traditional methods for doping macroscopic crystals are generally incompatible with the syntheses of such kinetically trapped nanostructures.[8−13] For example, a traditional method for preparation of high-quality crystals of II−VI semiconductor solid solutions is the Bridgman technique, in which the crystal growth front is in equilibrium with the melt reservoir and hence the crystal is formed at its thermodynamically favored composition. Heating colloidal nanocrystals to drive such equilibria usually results in severe Ostwald ripening and loss of the desired properties obtained from size or shape control. Consequently, efforts to dope nanocrystals have largely focused on impurity incorporation during growth, where doping is governed kinetically. Under these conditions, dopants must compete with host cations for available surface binding sites, and nanocrystal surfaces must compete against surfactant ligands for impurity binding. These surface competition reactions are biased against impurities that have mismatches in charge, size, geometry, ionicity, or other physical attributes and hence typically disfavor doping. For example, whereas bulk $Cd_{1-x}Mn_xSe$ crystals have been grown from the melt with x as high as 0.5,[15] synthesis of comparable colloidal $Cd_{1-x}Mn_xSe$ nanocrystals by state-of-the-art hot-injection methods has proven tremendously challenging.[11] Figure 1A adapts the Sugimoto model[14] of nutrient concentration gradients during crystal growth to describe the scenario of a small nanocrystal growing in the presence of both lattice nutrient and impurity ions. For $Cd_{1-x}Mn_xSe$ growth under normal hot-injection conditions, Cd^{2+} deposition is diffusion limited, resulting in depletion at the surfaces. Because of unfavorable hard/soft acid/base conditions, however, Mn^{2+} depletion at the same surface is negligible. The synthesis of colloidal $Cd_{1-x}Mn_xSe$ nanocrystals has therefore long served as a testing ground for the development of innovative nanocrystal

Received: July 15, 2013
Published: August 26, 2013

   dx.doi.org/10.1021/ja4072207 | J. Am. Chem. Soc. 2013, 135, 14380−14389

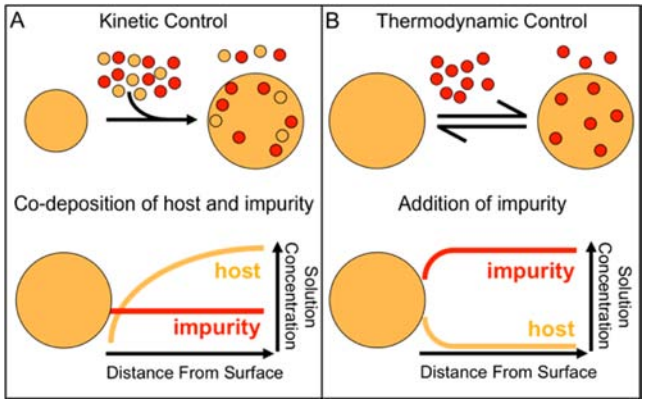

Figure 1. Incorporation of impurities into nanocrystals under (A) kinetic or (B) thermodynamic control. Under kinetic control, impurities compete with host nutrients for surface binding sites and are internalized via subsequent crystal lattice overgrowth. Under thermodynamic control, impurities enter the nanocrystal lattice under quasi-equilibrium conditions, driven by entropy, and are internalized via diffusion of the crystal ions.

doping chemistries intended to overcome these general challenges.

In specific cases, fast-diffusing ions can be introduced into colloidal nanocrystals at temperatures that are too low for substantial Ostwald ripening, allowing thermodynamic nanocrystal composition control.[16−25] The most thoroughly investigated of such chemistries is so-called "cation exchange".[16−22] A defining feature of cation-exchange reactions that makes them extremely powerful is that the anion sublattice remains invariant, allowing retention of crystallite shape anisotropies and phases despite dramatic changes in crystal composition. Under thermodynamic control, cation exchange is governed by the differences between crystal and solution chemical potentials (μ^{NC} vs $\mu^{solution}$) of the impurity and host ions. Unfortunately, such reactions are limited to a relatively small set of cation combinations for which diffusion is rapid. Raising temperatures to drive diffusion of less reactive cations such as Mn^{2+} can cause severe Ostwald ripening and sacrifice nanostructuring.[26] Mn^{2+} incorporation into magic-size ZnTe nanoclusters via cation exchange has been successful,[27] as has cation exchange in even smaller clusters,[28,29] but successful synthesis of $Cd_{1-x}Mn_xSe$ or related nanocrystals by cation exchange has not been reported. For example, deliberate attempts to introduce Mn^{2+} into preformed colloidal ZnSe nanocrystals at elevated temperatures were either unsuccessful[30] or accompanied by severe ripening and collapse of shape anisotropy.[26] Indeed, it has been a long-standing tenet of nanocrystal doping that Mn^{2+} diffusion in II−VI nanocrystals is negligible at normal colloid growth or handling temperatures and that equilibrium compositions are therefore inaccessible.[9,10,31,32] Researchers wishing to access the unique luminescent, magnetic, magneto-optical, or magneto-electronic properties of Mn^{2+}-doped II−VI semiconductor nanocrystals, or of other doped nanocrystals that do not involve fast diffusers, are thus to date primarily restricted to samples synthesized under kinetic control.

To achieve thermodynamically controlled Mn^{2+} doping of semiconductor nanocrystals, two seemingly incommensurate criteria must be met: the nanocrystals must be allowed to progress toward their equilibrium solid-solution composition without approaching their equilibrium morphology. In other words, the lattice must be sufficiently fluid to allow mixing rather than just heterostructure formation, but at the same time, interparticle (and in anisotropic crystals, also intraparticle) mass transfer must be avoided. Figure 1B illustrates the desired thermodynamically suppressed doping process, in this example via impurity addition to a preformed spherical nanocrystal. To be successful, the solution and lattice chemical potentials of both host and impurity ions must be tuned such that impurity addition is thermodynamically favorable and ripening is minimized. Simultaneously, it must provide sufficient thermal energy for impurity diffusion from the surfaces into the nanocrystal internal volumes.

Here we report development of a successful synthesis of high-quality colloidal $Cd_{1-x}Mn_xSe$ nanocrystals performed under thermodynamic rather than kinetic control, based on addressing the above challenges in a systematic way. Beginning with colloidal CdSe quantum dots prepared by state-of-the-art hot-injection methods, we demonstrate thermally activated diffusion of Mn^{2+} into the nanocrystal internal volumes. In contrast with cation-exchange processes described previously, we show that this diffusion doping involves stoichiometric cation + anion *addition*, without the loss of host cations, and hence increases the nanocrystal volume in proportion to x. In common with cation-exchange reactions, we show that this diffusion doping allows retention of the original nanocrystal size distributions, crystallographic phases, and even shape anisotropies. The resulting nanocrystals show Mn^{2+} concentrations exceeding any reported previously for colloidal $Cd_{1-x}Mn_xSe$ nanocrystals, while simultaneously showing size and shape uniformity unparalleled in doped CdSe nanocrystals to date. We then illustrate the generality of this method by describing doping of CdSe nanocrystals with other cationic impurities, sequential tandem doping of two impurities into the same CdSe nanocrystals, and preliminary results for diffusion doping of CdTe, CdS, and ZnSe nanocrystals. The materials reported here represent a new benchmark for high-quality doped CdSe nanocrystals in particular, and in general illustrate the value of diffusion doping for preparing complex doped nanostructures under thermodynamic control.

EXPERIMENTAL SECTION

Chemicals. Trioctylphosphine oxide (TOPO; 99%), 1-octadecene (ODE; 90%), hexadecylamine (HDA; 90%), Super-Hydride (1 M triethylborohydride in THF), tributylphosphine (TBP; 97%), oleylamine (70%), oleic acid (OA; 90%), selenium metal (99.99+%), tellurium metal (99.8%), CdO (99.99+%), $Cd(OAc)_2{\cdot}2H_2O$ (99.99+%), and $Fe(SO_4){\cdot}7H_2O$ (99+%) were purchased from Aldrich. Octadecylphosphonic acid (ODPA; 97%), trioctylphosphine (TOP; 97%), and $Mn(OAc)_2{\cdot}4H_2O$ (99.999+%) were purchased from Strem. Stearic acid (SA; 97%) was purchased from Acros. $Co(OAc)_2{\cdot}4H_2O$ was purchased from GFS chemicals. All chemicals were used as received.

Nanocrystal Synthesis and Diffusion Doping. Seed CdSe nanocrystals of different crystallographic phases, shapes, and sizes, as well as seed ZnSe, CdS, and CdTe nanocrystals, were all prepared by methods adapted from various literature sources[33−36] as described in detail in the Supporting Information. All nanocrystals have been capped with oleate prior to diffusion doping, but the complete elimination of the native ligands employed in the various syntheses is not assumed.

Diffusion doping of CdSe nanocrystals with Mn^{2+} was performed as follows: CdSe nanocrystals (~0.13 mmol in terms of CdSe units) were dried and added to 0.17 g (2.1 mmol) of selenium powder, 1 mL of ODE, and 1 mL of TBP in a septum-capped 5 mL round-bottom flask in a nitrogen-atmosphere glovebox. Separately, 12 g of ODE, 0.5 g of

dx.doi.org/10.1021/ja4072207 | J. Am. Chem. Soc. 2013, 135, 14380−14389

SA, and 1 g of HDA were added to a 100 mL three-neck round-bottom flask. Following heating of the latter solution for 30 min at 100 °C under vacuum, 0.03 g (0.1 mmol) of $Mn(OAc)_2{\cdot}4H_2O$ was added against a nitrogen overpressure. The flask was then placed under vacuum to remove acetic acid and water and then heated under nitrogen to 300 °C, at which point the CdSe/selenide solution was injected rapidly. This reaction mixture was held at temperatures between 290 and 300 °C for between a few seconds and 29 h. The reaction is aided by the greater activity of TBP than the more common TOP. As the solution was cooled to room temperature, 3 mL of toluene was added at ∼120 °C to prevent SA solidification. Parallel experiments in which the samples were heated to only 200 °C failed to incorporate Mn^{2+} (see the Supporting Information). The synthetic procedures for Co^{2+} or Fe^{2+} diffusion doping were identical, but with Co^{2+} added as $Co(OAc)_2{\cdot}4H_2O$ or Fe^{2+} added as $Fe(SO_4){\cdot}7H_2O$.

Diffusion doping of CdTe nanocrystals with Mn^{2+} was performed as follows: A 12 g portion of ODE, 1 g of HDA, and 0.5 g of SA were added to a 100 mL three-neck round-bottom flask. The solution was degassed for 30 min under vacuum at 100 °C and brought back under nitrogen. Under a nitrogen overpressure, 0.03 g (0.1 mmol) of $Mn(OAc)_2{\cdot}4H_2O$ was added, followed by a brief pump/purge cycle, before the solution was heated to 170 °C for the nanocrystal injection. In a separate, septum-capped 5 mL round-bottom flask, 0.32 g (2.5 mmol) of tellurium, 1 mL of TBP, 0.5 mL of 1 M Super-Hydride solution in THF, 1 mL of oleylamine, and CdTe (∼0.1 mmol in terms of CdTe units) nanocrystals were mixed in a nitrogen-atmosphere glovebox. This solution was injected into the Mn^{2+} solution at 170 °C and stirred for 30 min at this temperature.

All nanocrystals were washed using the same procedures: The nanocrystals were precipitated from solution by addition of ethanol and washed by repeated suspensions in toluene and flocculation with ethanol. In some cases, TOPO, HDA, OA, or TOP was added to improve nanocrystal solubility.

Physical Characterization. Room-temperature electronic absorption spectra were collected for colloidal toluene suspensions of nanocrystals in 0.1 cm path length cuvettes using a Cary 500 spectrophotometer (Varian). XRD data were collected from evaporated nanocrystal films on glass slides using a Bruker D8 Discover spectrometer at the University of Washington (UW) NanoTech User Facility. TEM samples were prepared by submerging a 200 mesh copper grid (Ted Pella, Inc.) in a 1 μM colloidal suspension of nanocrystals in toluene and allowing this substrate to dry in air. TEM images were obtained on an FEI TECNAI F20, 200 kV microscope at the UW NanoTech User Facility. Nanocrystal sizes and size distributions were determined by analysis of the images of >100 individual nanocrystals for each value reported. Relative atomic concentrations were obtained by analysis of dried nanocrystals digested in ultrapure nitric acid (EMD Chemicals) using inductively coupled plasma atomic emission spectrometry (ICP-AES; Perkin-Elmer). Room-temperature magnetic circular dichroism (MCD) spectra were collected on colloidal nanocrystal suspensions in a 0.1 cm path length cuvette placed in a 1.5 T electromagnet oriented in the Faraday configuration. Low-temperature absorption and MCD spectra were collected on nanocrystal films prepared by depositing dilute toluene suspensions between two quartz disks. These samples were placed in a superconducting magneto-optical cryostat (Cryo-Industries SMC-1659 OVT) oriented in the Faraday configuration. At helium temperature, each sample was screened for depolarization by matching the CD spectra of a chiral molecule placed before and after the sample. In all cases, depolarization was <5%. Electronic absorption and MCD spectra were collected simultaneously using an Aviv 40DS spectropolarimeter. The differential absorption collected in the MCD experiment is reported as $\Delta A = A_L - A_R$, where A_L and A_R refer to the absorption of left and right circularly polarized photons in the sign convention of Piepho and Schatz.[37,38] From these data, values of ΔE_{Zeeman} and g_{Exc} can be obtained.[12,39]

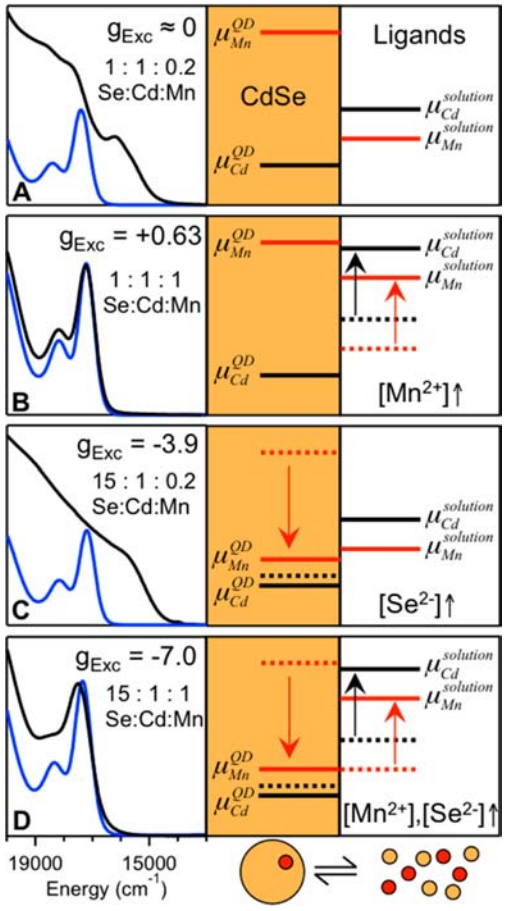

Figure 2. (Left) Room-temperature electronic absorption spectra of the first excitonic feature of zb-CdSe nanocrystals before (blue) and after (black) 30 min at 300 °C under the conditions described in the text and with the ion ratios indicated. Undoped zb-CdSe nanocrystals are injected into reaction solutions with (A) Mn^{2+} in a 0.2:1 ratio to the Cd^{2+} contained in the nanocrystals, (B) Mn^{2+} in solution in a 1:1 ratio with the Cd^{2+} contained in the nanocrystals, (C) Se^{2-} and Mn^{2+} in a 15:1 and 0.2:1 ratios to the Cd^{2+} contained in the nanocrystals, and (D) Se^{2-} and Mn^{2+} in a 15:1:1 ratio to the Cd^{2+} contained in the nanocrystals. The excitonic g values of the resulting nanocrystals, determined from room-temperature MCD spectroscopy, are given in each panel and indicate negligible-to-weak Mn^{2+}–exciton exchange coupling in panels A and B and strong exchange coupling in panels C and D. (Right) Relative free energies of the Mn^{2+} and Cd^{2+} cation chemical potentials on either side of the nanocrystal/solution interface for identical reaction conditions with the exception of relative ionic ratios.

RESULTS AND ANALYSIS

Figure 2 summarizes results from a series of experiments performed to elucidate the roles of Mn^{2+} and Se^{2-} concentrations in diffusion doping. Room-temperature absorption and MCD spectra were used as convenient probes for monitoring sample evolution under various diffusion-doping conditions. For the baseline experiment, presented in Figure 2A, experimental conditions resemble those of a typical hot-injection synthesis during postnucleation growth, in which the ratio of Mn^{2+} (solvated) to Cd^{2+} (as CdSe seed nanocrystals) is relatively small (0.2:1) and no excess Se^{2-} has been added. Prior to heating, the seed nanocrystals show a narrow exciton peak at ∼17 500 cm^{-1}. After heating, the absorption spectrum is broadened substantially and shifted to lower energy,

dx.doi.org/10.1021/ja4072207 | J. Am. Chem. Soc. 2013, 135, 14380–14389

indicative of severe Ostwald ripening and loss of size uniformity. The room-temperature MCD spectrum shows no evidence of substantial Mn^{2+} incorporation. As detailed previously,[11,12,40,41] doping CdSe nanocrystals with Mn^{2+} results in MCD intensity inversion and enhancement at the CdSe absorption edge. These changes arise from the introduction of strong sp−d exchange contributions to excitonic Zeeman splittings upon Mn^{2+} doping, as described by eq 1.[12,39] The first term in eq 1 describes the intrinsic

$$\Delta E_{\text{Zeeman}} = g_{\text{int}}\mu_{\text{B}}B + x_{\text{eff}}\langle S_z\rangle N_0(\alpha - \beta) \quad (1)$$

contribution to the excitonic Zeeman splitting energies (ΔE_{Zeeman}) of CdSe nanocrystals. This contribution is small, temperature independent, and linearly dependent on the magnetic field (B, where μ_{B} is the Bohr magneton). Experimental measurements have yielded $g_{\text{int}} \approx +1$ for undoped pseudospherical CdSe nanocrystals.[40,42] The second term in eq 1 describes the dopant−exciton sp−d exchange coupling contribution to ΔE_{Zeeman}, where $\langle S_z\rangle$ is the spin expectation value of the dopant at the experimental temperature and magnetic field (as described by the Brillouin function for magnetic ions with spin-only ground states, such as Mn^{2+}), $N_0(\alpha-\beta)$ is the mean-field sp−d exchange energy, and x_{eff} represents the effective amount of paramagnetic Mn^{2+} exchange coupled with the exciton. $\langle S_z\rangle$ is strongly temperature dependent, increasing as $1/T$ for simple paramagnets such as Mn^{2+}. x_{eff} is generally smaller than x because of Mn^{2+}−Mn^{2+} pair formation,[15,43] reaching its maximum of ∼3.3% when x is ∼8.2%. In nanocrystals, x_{eff} is typically also smaller than x because of undoped cores.[44,45] For the cases studied here, the sp−d exchange term has the opposite sign compared to the intrinsic term. In the limit of small B, $\langle S_z\rangle$ is also linearly proportional to B (the Curie limit). In this regime, the proportionality constant $g_{\text{Exc}} = \Delta E_{\text{Zeeman}}/\mu_{\text{B}}B$ provides a measure of these two competing contributions to ΔE_{Zeeman}. For the purposes of this study we consider negative g_{Exc} values to be indicative of substantial Mn^{2+} incorporation and positive g_{Exc} values as indicative of an absence of such incorporation, although positive g_{Exc} values can be obtained at high temperatures in doped nanocrystals with low doping concentrations.[46] Room-temperature MCD spectroscopy of the nanocrystals in Figure 2A shows little or no intensity at the first exciton, $g_{\text{Exc}} \approx 0$, and hence little or no success in doping.

Figure 2A (right) illustrates why doping fails here, in terms of Cd^{2+} and Mn^{2+} chemical potentials. Under these experimental conditions, the soft Cd^{2+} Lewis acid preferentially binds to the soft Se^{2-} rather than to the hard Lewis bases present in solution as surfactants (stearate and hexadecylamine). Conversely, Mn^{2+} prefers these harder ligands. The resulting imbalance in chemical potentials favors Mn^{2+} solvation and is responsible for the unsuccessful exchange of Cd^{2+} by Mn^{2+} under these conditions. Moreover, the relatively small imbalance between $\mu_{\text{Cd}}^{\text{NC}}$ and $\mu_{\text{Cd}}^{\text{solution}}$ allows large Cd^{2+} diffusion lengths in solution and hence Ostwald ripening.

To encourage doping, the Mn^{2+} concentration in solution was increased massively relative to the conditions of Figure 2A so that it equaled the total Cd^{2+} content of the seed CdSe nanocrystals. These levels more closely resemble conditions in cation-exchange reactions than in kinetic doping reactions. Figure 2B (left) shows absorption spectra collected before and after heating CdSe nanocrystals in the presence of such an excess of Mn^{2+}. A positive value of $g_{\text{Exc}} = +0.63$ is observed by MCD spectroscopy following heating at 300 °C for 30 min, again indicating little or no successful doping. Although Mn^{2+} is not incorporated, the nanocrystals remarkably preserve their average size and narrow size distribution despite prolonged heating. These observations can be understood by considering the effects of increased Mn^{2+} concentration illustrated in Figure 2B (right). When Mn^{2+} is added as $Mn(OAc)_2$, its ligands can be exchanged by pumping off acetic acid, such that Mn^{2+} in the reaction solution is coordinated by the surfactant ligands, stearate and hexadecylamine. Such a large increase in Mn^{2+} concentration thus increases the chemical potentials of both Mn^{2+} and Cd^{2+} ions in solution because the free ligand concentration decreases (analogous to the common-ion effect). Supporting this interpretation, control experiments confirm that adding more HDA increases Ostwald ripening again. The added driving force for Cd^{2+} binding to the CdSe surfaces offsets any increased driving force for Mn^{2+} incorporation into the crystals, and consequently, doping does not proceed. At the same time, the increased chemical potential of Cd^{2+} in solution attenuates CdSe diffusion and thereby suppresses Ostwald ripening.

For successful doping, the CdSe nanocrystal surface must be made more attractive for Mn^{2+} binding. Figure 2C (left) shows absorption spectra collected before and after heating when excess Se^{2-} (instead of excess Mn^{2+}) is added at a 15:1 ratio to total Cd^{2+}, with other conditions the same as in Figure 2A. Upon heating, the CdSe absorption edge red shifts by ∼1500 cm^{-1} and broadens considerably, indicating extensive ripening, but room-temperature MCD spectra of the resulting nanocrystals show sign inversion and yield $g_{\text{Exc}} = -3.9$, indicating dominance of Mn^{2+}−exciton sp−d exchange and hence successful Mn^{2+} incorporation. Figure 2C (right) illustrates the origins of these changes. With excess Se^{2-}, the Mn^{2+} chemical potential inside the lattice drops to a level where solid-solution formation is thermodynamically favorable. Mn^{2+} adds to the lattice not by expulsion of Cd^{2+}, but via incorporation of new Mn−Se units instead. This feature constitutes an essential distinction between the diffusion-doping process reported here and previous cation-exchange chemistries.

By combining the suppression of Ostwald ripening at high Mn^{2+} concentrations (Figure 2B) with the elimination of cation competition for Se^{2-} at high Se^{2-} concentrations (Figure 2C), diffusion doping of CdSe nanocrystals to form $Cd_{1-x}Mn_xSe$ nanocrystals could be optimized. Figure 2D (left) shows absorption spectra collected before and after heating CdSe seed nanocrystals at 300 °C for 30 min in the presence of high concentrations of excess Se^{2-} and excess Mn^{2+}. Instead of a red shift from Ostwald ripening, the first CdSe excitonic maximum blue shifts and broadens slightly. Furthermore, room-temperature MCD spectroscopy yields $g_{\text{Exc}} = -7.0$ for these nanocrystals after heating, indicative of very strong sp−d exchange and hence of even more successful doping than in Figure 2C. As illustrated in Figure 2D (right), the chemical potentials of both Cd^{2+} and Mn^{2+} decrease inside the CdSe nanocrystals and increase in solution when both are added in excess. Importantly, neither XRD nor TEM shows any suggestion of MnSe formation under the conditions of Figure 2D (vide infra), from which we conclude that this phase either does not form at all or exists only as an intermediate. Control experiments performed in the absence of seed CdSe nanocrystals also fail to produce MnSe.

dx.doi.org/10.1021/ja4072207 | J. Am. Chem. Soc. 2013, 135, 14380−14389

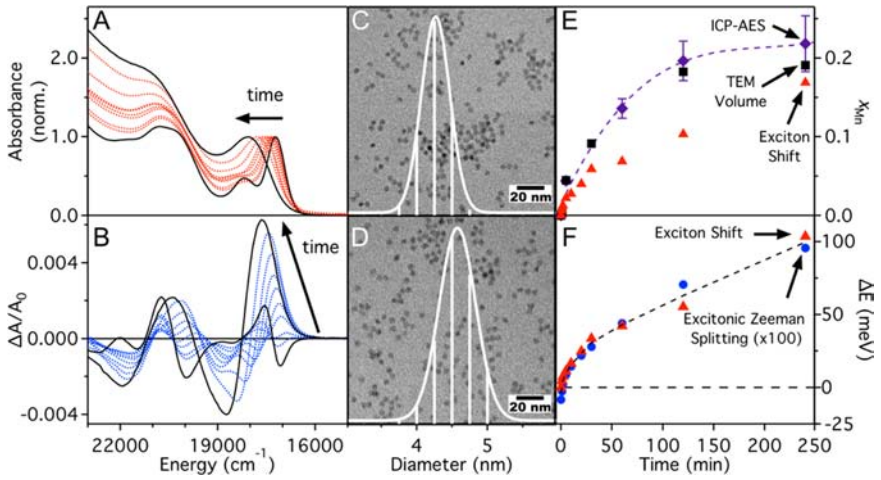

Figure 3. (A) Room-temperature electronic absorption spectra of reaction aliquots taken at different times during w-CdSe nanocrystal diffusion doping at 300 °C, normalized at the first excitonic maximum. (B) Corresponding MCD spectra showing a sign inversion and signal growth with increased reaction time, indicative of growing sp−d exchange coupling strengths. (C) TEM image and corresponding diameter histogram from analysis of undoped CdSe (d = 4.37 ± 0.18 nm) precursor nanocrystals. (D) TEM image and corresponding diameter histogram from analysis of $Cd_{1-x}Mn_xSe$ nanocrystals after 240 min of diffusion doping at 300 °C (d = 4.69 ± 0.24 nm). (E) Mn^{2+} cation mole fraction (x_{Mn}) determined by ICP-AES (purple tilted squares, with error bars from three measurements of each aliquot), analysis of nanocrystal volumes from TEM (black squares), and analysis of the excitonic absorption energy shifts (red triangles). The dashed line is a guide to the eye. In order of increasing reaction time, the standard deviations on the average nanocrystal diameters from TEM are 4.1% (seed), 3.4%, 4.1%, 3.8%, 3.6%, and 5.1% (see the Supporting Information). (F) Excitonic absorption energy shifts (red triangles, from analysis of panel A data) and excitonic Zeeman splittings (blue circles, from analysis of panel B data, multiplied by 100) plotted vs the diffusion-doping time. The dashed line is a guide to the eye. See the text and Supporting Information for additional details.

The data in Figure 2D are interpreted as reflecting Mn−Se addition to and diffusion into the seed CdSe nanocrystals. To explore the chemistry of Figure 2D in more depth, a reaction was performed under the same optimized conditions and aliquots were removed periodically. Figure 3A shows the evolution of the CdSe absorption spectrum with the reaction time at 300 °C. The first excitonic feature broadens and shifts to higher energy as the reaction proceeds. Figure 3B shows that this trend is accompanied by an inversion and progressive increase in MCD intensity at the CdSe absorption edge. g_{Exc} becomes dominated by sp−d exchange within only ∼2 min. These data are consistent with rapid Mn^{2+} incorporation into the CdSe nanocrystals and a growing x_{eff} (eq 1) throughout the entire reaction.

Figure 3C shows a TEM image of the seed CdSe nanocrystals used in the experiments of Figure 3A,B. These nanocrystals have a diameter of 4.37 ± 0.18 nm (σ = 4.1%). Figure 3D shows a TEM image of the same nanocrystals after 4 h of heating at 300 °C in the presence of excess Mn^{2+} and Se^{2-}. The average diameter increases to 4.69 ± 0.24 nm (σ = 5.1%). We attribute this growth entirely to addition of Mn−Se units to the seed CdSe nanocrystal. From this volume increase, a value of $x_{Mn} \approx 0.19$ can be inferred in the maximally doped nanocrystals, corresponding to ∼195 Mn^{2+} ions/nanocrystal. Similar analyses were performed for other aliquots (Supporting Information). Figure 3E summarizes the TEM results, plotting the data as x_{Mn} vs diffusion-doping time under the assumption that growth derives solely from addition of Mn−Se units. These data show an initial increase and subsequent plateau at $x_{Mn} \approx 0.19$ over the course of 4 h. This curvature is indicative of an equilibrium process. For comparison, x_{Mn} was also determined analytically for each aliquot using ICP-AES following careful washing to remove adventitious Mn^{2+}. Figure 3E plots these analytical concentrations on the same axes as the concentrations estimated from TEM. The analytical x_{Mn} data agree very well with the values deduced from the TEM data, again increasing over the first 2 h before plateauing at $x_{Mn} \approx 0.22$. The agreement between these two data sets confirms that this synthesis introduces Mn^{2+} into seed CdSe nanocrystals by addition of Mn−Se units. Beyond this unprecedentedly large Mn^{2+} concentration in colloidal CdSe nanocrystals, the remarkable feature of these data is that the nanocrystal size distribution remains essentially unchanged following such prolonged heating.

The TEM results show that the exciton broadening seen in Figures 2D and 3A does not come from a loss of the size uniformity. Instead, this broadening reflects perturbation of the transition energy due to Mn^{2+} addition. Figure 3F plots the energy of the first excitonic maximum (E_g) vs Mn^{2+} diffusion-doping time for the same aliquots. E_g *increases* with Mn^{2+} addition, despite the increasing nanocrystal volumes. This increase starts immediately and proceeds for the first 2 h before leveling somewhat, but a terminal plateau is not reached within 4 h. These data demonstrate that Mn−Se does not simply deposit onto the CdSe NC surfaces to form CdSe/MnSe core/shell structures. Like CdSe/ZnSe core/shell nanocrystals, such structures would show exciton relaxation into the shell layer and hence a small decrease in E_g. Instead, the data confirm $Cd_{1-x}Mn_xSe$ solid-solution formation. To understand these data, we recall that E_g in bulk CdSe displays a well-defined dependence on x_{Mn}, shifting to higher energy linearly with a slope of ∼+11.4 meV/x_{Mn} (%) (or +92 cm^{-1}/x_{Mn} (%)).[39] This shift is largely attributable to the fact that the empty Mn^{2+} 4s orbitals are in poor energetic alignment with the Cd^{2+} 5s orbitals,[47,48] and consequently, Mn^{2+} inclusion into the lattice disrupts the CdSe conduction band. The blue shift in E_g with increasing nanocrystal volume shown in Figure 3 thus results from the dependence of E_g on x_{Mn}. An estimate of x_{Mn} from E_g was attempted but is made difficult by the fact that these nanocrystals are quantum confined, and addition of Mn−Se

dx.doi.org/10.1021/ja4072207 | J. Am. Chem. Soc. 2013, 135, 14380−14389

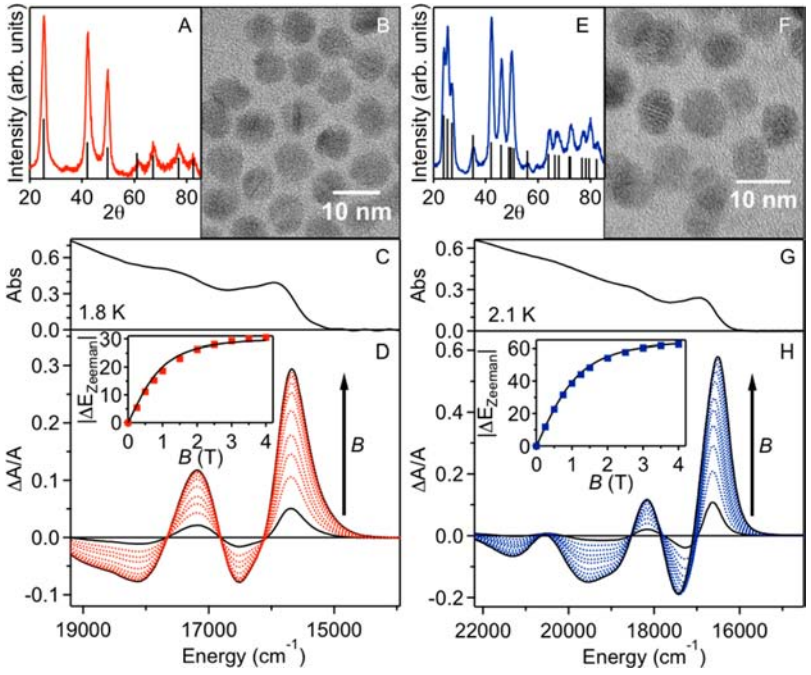

Figure 4. (A) XRD and (B) TEM data for the $d = 8.8 \pm 0.8$ nm zb-$Cd_{1-x}Mn_xSe$ nanocrystal product obtained from diffusion doping of $d = 8.4$ nm zb-CdSe precursor nanocrystals for 30 min as in Figure 2D. (C, D) Electronic absorption (C) and variable-field MCD (D) spectra (1.8 K) of $d = 8.4$ nm zb-$Cd_{1-x}Mn_xSe$ nanocrystals. (E) XRD and (F) TEM data for the $d = 7.9 \pm 0.5$ nm w-$Cd_{1-x}Mn_xSe$ nanocrystal product obtained from diffusion doping of 6.8 nm w-CdSe seed nanocrystals. (G, H) Electronic absorption (G) and variable-field MCD (H) spectra (2.1 K) of $d = 7.9$ nm w-$Cd_{1-x}Mn_xSe$ nanocrystals. The insets to (D) and (H) plot the excitonic Zeeman splittings vs magnetic field, deduced from the MCD spectra. The solid curves plot $S = 5/2$ Brillouin functions calculated using $g_{Mn} = 2.0$ and the experimental temperatures. At saturation, $\Delta E_{Zeeman} = -31$ and -65 meV for these zinc blende and wurtzite $Cd_{1-x}Mn_xSe$ nanocrystals, respectively. The excitonic g values in the limit of small magnetic fields are $g_{Exc} = -376$ and -815 for the zinc blende and wurtzite $Cd_{1-x}Mn_xSe$ nanocrystals, respectively.

units simultaneously relaxes the exciton spatial confinement. If we assume that E_g simply scales linearly with x_{Mn} as in the bulk, but now starts from E_g of the undoped CdSe NCs and finishes at the bulk band gap energy of the hypothetical wurtzite MnSe (i.e., assuming no MnSe quantum confinement at these diameters and no relaxation of confinement with Mn−Se addition to CdSe nanocrystals), then the excitonic blue shift in Figure 3F implies a value of $x_{Mn} \approx 0.14$. Taking into account the increasing nanocrystal volumes determined by TEM, the excitonic shift data can be corrected for the relaxation of quantum confinement in the CdSe host[35,49] to yield a final $x_{Mn} \approx 0.17$ (Figure 3E), which agrees well with the values determined by ICP-AES and from TEM volume increases. For comparison with the absorption data, Figure 3F also shows the room-temperature excitonic Zeeman splitting energies (ΔE_{Zeeman}) determined from analysis of the MCD intensities in Figure 3B, plotted vs diffusion-doping time. These data behave in essentially the same way as E_g. The fact that Mn^{2+} addition plateaus (Figure 3E) but the spectroscopic effects of Mn^{2+} continue to increase (Figure 3F) provides strong evidence for a mechanism involving initial Mn−Se deposition within an active surface volume, followed by slower homogenization of the $Cd_{1-x}Mn_xSe$ solid solution.

To test whether diffusion doping retains the crystallographic phase, samples of predominantly hexagonal wurtzite (w) or cubic zinc blende (zb) CdSe nanocrystals were reacted with Mn^{2+} under identical conditions. The different crystal phases of these samples derive from different synthesis conditions (see the Supporting Information), but under the identical diffusion-doping reaction conditions, both samples should have the same thermodynamically favored crystal phase.

Figure 4A−D shows data collected following 30 min of diffusion doping of $d = 8.4$ nm zb-CdSe seed nanocrystals under the same optimized conditions as in Figure 2D. The TEM data of Figure 4B show growth to $d = 8.8$ nm, and the XRD data of Figure 4A show retention of the cubic lattice structure. Likewise, Figure 4E−H show data collected following 60 min of diffusion doping of $d = 6.8$ nm w-CdSe seed nanocrystals under the same conditions. The TEM data of Figure 4F show growth to $d = 7.9$ nm, and the XRD data of Figure 4E show retention of the wurtzite lattice structure. From the XRD peak positions and bulk relationships between x_{Mn} and XRD peak positions, x_{Mn} values of 0.12 ± 0.02 and 0.19 ± 0.01 are estimated for the zinc blende and wurtzite $Cd_{1-x}Mn_xSe$ nanocrystals, respectively, consistent with the results of Figure 3.[15]

Parts C and D and parts G and H of Figure 4 plot low-temperature absorption and variable-field MCD spectra of these nanocrystals after diffusion doping. In both cases, the MCD signals are very strong and show the hallmark signatures of successful Mn^{2+} doping. Plots of ΔE_{Zeeman} vs magnetic field (insets) show the $S = 5/2$ saturation magnetization expected for $Cd_{1-x}Mn_xSe$. For the zb-$Cd_{1-x}Mn_xSe$ nanocrystals, ΔE_{Zeeman} saturates at -31 meV and $g_{Exc} = -376$ in the low-field limit (1.8 K). For the w-$Cd_{1-x}Mn_xSe$ nanocrystals, ΔE_{Zeeman} saturates at -65 meV and $g_{Exc} = -815$ in the low-field limit (2.1 K), consistent with their greater x_{Mn}. The largest ΔE_{Zeeman} we have achieved using diffusion doping is $\Delta E_{Zeeman} = -100$ meV, with an extraordinarily large value of $g_{Exc} = -907$ (at 1.8 K; see the Supporting Information). This ΔE_{Zeeman} value is close to the maximum of -120 meV anticipated from bulk sp−d exchange parameters and the maximum x_{eff} of ~3.3%.[43] Comparison with

dx.doi.org/10.1021/ja4072207 | J. Am. Chem. Soc. 2013, 135, 14380−14389

the literature shows these to be the largest magneto-optical effects achieved for $Cd_{1-x}Mn_xSe$ nanocrystals of any type to date, for example, exceeding the next largest ΔE_{Zeeman} and g_{Exc} values by nearly a factor of 2.[11,12] Such strong magneto-optical responses, and the magneto-electronic properties they report upon, constitute one of the main motivations for synthesis of this class of materials. Beyond showing that diffusion doping yields high-quality $Cd_{1-x}Mn_xSe$ nanocrystals with record large magneto-optical effects, the results in Figure 4 demonstrate that diffusion doping retains the crystallographic phases of the seed nanocrystals, a key finding.

To test whether diffusion doping also retains the nanocrystal shape, experiments were performed using anisotropic seed nanocrystals. Figure 5A shows TEM data of CdSe nanorods

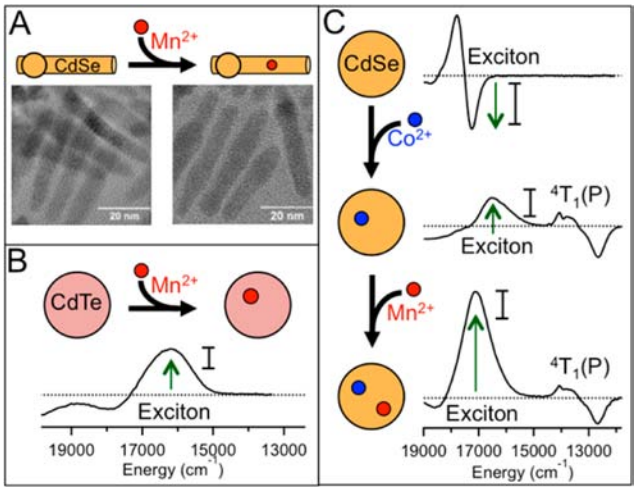

Figure 5. (A) Diffusion doping of seeded w-CdSe nanorods. TEM images collected before and after diffusion doping of seeded CdSe nanorods ($d \approx 6-8$ nm, aspect ratio ~6:1) with Mn^{2+} at 300 °C for 30 min. The nanorods retain their shapes. MCD spectra confirm doping (see the Supporting Information). (B) MCD spectrum of CdTe nanocrystals after diffusion doping with Mn^{2+}, showing inversion of the excitonic MCD signal indicative of successful doping. (C) Tandem diffusion doping of zb-CdSe nanocrystals with Co^{2+} followed by Mn^{2+}. (Top) MCD of undoped CdSe precursor nanocrystals. (Middle) MCD spectrum of the same nanocrystals after diffusion doping with Co^{2+}, showing inversion of the excitonic MCD signal and appearance of the characteristic Co^{2+} $^4T_1(P)$ d−d transition. (Bottom) MCD spectrum of the same nanocrystals following diffusion doping with Mn^{2+}, showing increased excitonic Zeeman splitting and retention of the Co^{2+} $^4T_1(P)$ d−d transition. The vertical scale bars indicate intensities of $\Delta A/A_0 = 0.001$. All MCD spectra were collected at 300 K.

prepared by seeded growth and having $d \approx 6-8$ nm with ~6:1 aspect ratios and distinct bulges that are characteristic of seeded-growth nanorods.[34] The shapes, sizes, and even bulges of these nanorods are retained following 30 min of diffusion doping with Mn^{2+} at 300 °C under the optimized conditions of Figure 2D, with successful doping confirmed by MCD spectroscopy (see the Supporting Information). Combined, the above results demonstrate diffusion doping as a new example of nanocrystal composition control without loss of crystallographic phase, size uniformity, or shape anisotropy, placing this method alongside cation exchange in these capacities.

Although the present work has focused primarily on optimization of reaction conditions for the benchmark $Cd_{1-x}Mn_xSe$ nanocrystal system, the principles underpinning the diffusion-doping process described here are general, and the chemistry should therefore also be broadly generalizable. For example, by replacing CdSe nanocrystals and Se^{2-} with CdTe nanocrystals and Te^{2-}, decreasing the injection temperature to 170 °C, and adding a reductant (Super-Hydride) to accommodate the lower stability of Te^{2-} in solution,[50] successful synthesis of $Cd_{1-x}Mn_xTe$ nanocrystals was achieved (Figure 5B) but without satisfactory suppression of Ostwald ripening, as in Figure 2C. Similar preliminary results have been obtained for $Cd_{1-x}Mn_xS$ and $Zn_{1-x}Mn_xSe$ nanocrystals (Supporting Information). Doping by addition thus appears broadly promising, and we speculate that with optimization it should also be possible to suppress Ostwald ripening to the same extent in these cases as in the $Cd_{1-x}Mn_xSe$ syntheses discussed above. Optimization within each of these large parameter spaces was considered beyond the scope of the present study.

Extension of this diffusion-doping synthesis to other cations has also been preliminarily investigated. Hard Lewis acids such as Al^{3+}, Mg^{2+}, Gd^{3+}, and Er^{3+} were found to bind the capping ligands too strongly and cause sample precipitation. Attempts to codope these ions simultaneously with Mn^{2+}, thereby using a lower concentration of the interfering ion, sacrificed the ability of Mn^{2+} to suppress Ostwald ripening, likely for the same reason. Extension of this method to these hard Lewis acids may be possible with identification of a suitable ligand set, but this parameter space has not yet been thoroughly explored. On the other end of the spectrum, extension to soft Lewis acids such as Cu^+ and Ag^+ was not possible because of rapid formation of their respective selenide lattices separately from the CdSe nanocrystals. Cation-exchange reactions involving these cations avoid such competing side reactions by not including excess anion, and indeed, the new method introduced here can be considered unnecessary for these ions. Borderline hard/soft Lewis acids were also examined: Replacing Mn^{2+} with excess Fe^{2+} without excess Se^{2-} was found to successfully preserve the absorption spectrum of the seed CdSe nanocrystals (see the Supporting Information), precisely as with Mn^{2+} in Figure 2B. Importantly, the nanocrystals also retain their excitonic photoluminescence. Fe^{2+} is a "killer trap" for luminescence in II−VI semiconductors, and this result thus indicates an absence of Fe^{2+} doping in the absence of excess Se^{2-} (as concluded for Mn^{2+} above). Addition of Se^{2-} to this reaction mixture leads to an increase in E_g with reaction time and complete quenching of the CdSe luminescence (see the Supporting Information), consistent with successful Fe^{2+} incorporation. Fe^{2+} diffusion doping into CdSe nanocrystals thus closely mirrors that of Mn^{2+}. Similarly, using Co^{2+} in place of Mn^{2+} allows the successful synthesis of $Cd_{1-x}Co_xSe$ nanocrystals with high Co^{2+} concentrations (see below and the Supporting Information).

Finally, the capacity to separate doping from nanocrystal synthesis introduces new opportunities to prepare doped nanostructures that would be difficult to obtain under kinetic trapping conditions. For example, previous work has shown that dopants are excluded from very small semiconductor nanocrystals under kinetic doping conditions.[9,44,45,51] Among other things, this behavior has complicated the analysis of the recently discovered intrinsic dual emission phenomenon in small $Cd_{1-x}Mn_xSe$ nanocrystals because of the coexistence of both doped and undoped nanocrystals.[52] To overcome this problem, $Cd_{1-x-y}Zn_xMn_ySe$ alloys and complex $Zn_{1-x}Mn_xSe$/CdSe and $Zn_{1-x}Mn_xSe$/ZnS/CdS/ZnS nanocrystal hetero-

dx.doi.org/10.1021/ja4072207 | J. Am. Chem. Soc. 2013, 135, 14380−14389

structures were developed.[53−55] By diffusion doping, we have now succeeded in reaching large values of x_{Mn} in CdSe nanocrystals small enough to show pronounced dual emission directly in $Cd_{1-x}Mn_xSe$ for the first time, without signal contamination from undoped nanocrystals (see the Supporting Information), and have also successfully added both Mn^{2+} and Zn^{2+} into seed CdSe nanocrystals in one simultaneous step, offering a convenient new way to achieve dual-emitting nanocrystals. Furthermore, qualitatively new chemistries are now possible. For example, Figure 5C shows excitonic MCD spectra of d = 3.8 nm CdSe seed nanocrystals that are doped sequentially by addition of Co^{2+} and then Mn^{2+}. The undoped CdSe nanocrystals show a negative leading-edge MCD intensity consistent with the absence of sp−d exchange. Diffusion doping with Co^{2+} for 30 min at 300 °C inverts the excitonic MCD signal and yields the characteristic Co^{2+} $^4A_2(F) \rightarrow {}^4T_1(P)$ MCD feature centered at 13 370 cm^{-1}, confirming successful incorporation of Co^{2+} at the tetrahedral cation sites of the CdSe lattice.[40,41] After subsequent diffusion doping with Mn^{2+} for 40 min at 300 °C, the Co^{2+} $^4A_2(F) \rightarrow {}^4T_1(P)$ transition is retained and the excitonic MCD intensity is further increased. The ratio of excitonic to Co^{2+} ligand-field absorbance varies slowly during Mn^{2+} incorporation (see the Supporting Information), indicating minimal loss of Co^{2+} during Mn^{2+} addition, consistent with the large difference between lattice and solution chemical potentials for all cations under these conditions.

DISCUSSION

The data presented here reveal the remarkable ability to introduce Mn^{2+} into high-quality hot-injection CdSe nanocrystals from very low to exceptionally high values of x_{Mn} simply by changing the reaction time, without sacrificing the nanocrystal size or shape uniformity or the crystallographic phase. This process is reminiscent of cation exchange in nanocrystals, but displays a few key differences. First, to date it has been a general requirement of nanocrystal cation-exchange reactions that the participating cations diffuse rapidly. The chemistry demonstrated here involves Mn^{2+}, which shows negligible diffusion into II−VI semiconductor nanocrystals at room temperature. Instead, this diffusion must be activated thermally, requiring long incubation at relatively high temperatures that would normally also cause severe Ostwald ripening. Second, it is a fundamental property of nanocrystal cation-exchange reactions that the number of anions per nanocrystal is invariant,[16] but the results presented above demonstrate that this diffusion doping involves stoichiometric anion and cation *addition*. The data suggest rapid composition equilibration at the surfaces followed by slower cation randomization within the nanocrystals' internal volumes, precisely how cation exchange proceeds at bulk II−VI semiconductor surfaces,[56] but this stoichiometric cation + anion addition avoids the need to eject Cd^{2+} to form less favorable Mn^{2+}−Se^{2-} bonds. This feature represents a defining characteristic of the diffusion doping presented here that differentiates it from cation-exchange chemistries explored previously.[16−22] Because of this qualitative difference, diffusion doping provides the opportunity to introduce relatively unreactive cations such as Mn^{2+} into semiconductor nanocrystals such as CdSe that have been notoriously difficult to dope under kinetic control. Sequential tandem doping has been used to illustrate the qualitative difference between this doping by addition and previous cation-exchange or kinetic trapping chemistries. Despite these differences, diffusion doping also offers some of the most attractive features of cation exchange, namely, retention of seed nanocrystal shape anisotropies, sizes and size distributions, and crystallographic phases. These properties identify diffusion doping as a valuable new addition to our current repertoire of methods for controlling crystal composition at the nanoscale.

Scheme 1

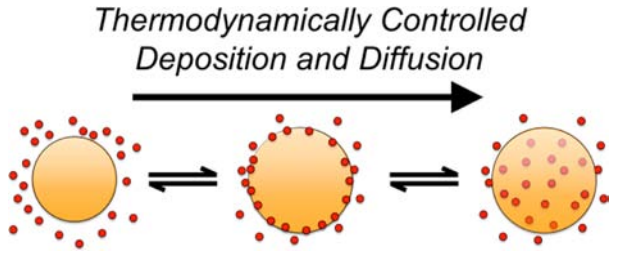

Scheme 1 summarizes the diffusion-doping chemistry found here, illustrating a case of doping spherical nanocrystals. Surface binding equilibria, defined by the relative solution vs lattice chemical potentials of the host and impurity cations, allow the thermodynamic solid-solution compositions to be reached within an effective reaction volume at the nanocrystal surfaces (Figure 3E). This equilibration is followed on a longer time scale (Figure 3F) by impurity randomization within the nanocrystal internal volumes. Ostwald ripening is suppressed despite the long reaction times at high temperatures because of the limited availability of uncoordinated surfactant ligands and the ample availability of lattice anions. These two factors minimize the solution diffusion length of the host cations.

Although interparticle Cd^{2+} diffusion can be successfully minimized, Cd^{2+} ions continue to diffuse at the nanocrystal surfaces. Surface diffusion is essential for the formation of solid-solution $Cd_{1-x}Mn_xSe$ nanocrystals rather than simple core/shell CdSe/MnSe nanocrystals. As in cation exchange, this reactive surface layer must be small compared to the dimensions of the nanocrystals themselves for the crystallographic phases and shape anisotropies of the seed nanocrystals to be preserved.[16]

The chemical trends in diffusion doping observed here can be understood by considering the surface equilibria as governed by hard/soft acid/base rules. The experimental conditions identified here (including cation, anion, ligand, and nanocrystal concentrations, as well as temperature) were optimized for introduction of Mn^{2+} into CdSe nanocrystals and subsequently found to be suitable for introduction of Fe^{2+} and Co^{2+} as well. These cations share in common that they are all borderline hard Lewis acids. By contrast, more conventional cation-exchange chemistries excel when using soft Lewis acids (e.g., Cu^+, Ag^+, Au^+, Cd^{2+}, Pb^{2+}, and Hg^{2+}), which have a greater affinity for the lattice anions and hence can more easily displace the initial host cations. For the same reason, use of these soft cations under the present diffusion-doping conditions simply leads to nucleation of their independent phases because of the large excess ion concentrations used. Conditions for doping hard Lewis acids (e.g., Al^{3+}, trivalent lanthanides) into II−VI semiconductors via diffusion have so far not been identified but should exist. Under the present conditions, such hard Lewis acids have too great an affinity for the hard surfactant Lewis bases employed.

Essential to the success of this diffusion-doping strategy in the present case is the fact that MnSe crystallites do not form

dx.doi.org/10.1021/ja4072207 | J. Am. Chem. Soc. 2013, 135, 14380−14389

under the experimental reaction conditions. Formation of MnSe nanoclusters has been reported under conditions similar to those used here,[57] but with the key differences that the present reaction mixtures (i) contain nearly an order of magnitude more stearic acid relative to Mn^{2+} and (ii) also contain CdSe nanocrystals. Both of these additions disfavor MnSe formation by introducing processes that compete for available Mn^{2+} (ligation and surface binding, respectively). The presence of excess stearic acid makes MnSe formation unfavorable.

This synthesis of $Cd_{1-x}Mn_xSe$ nanocrystals is distinct from any reported previously, but its comparison to analogous chemistries is instructive. One interesting analogue is the conversion of CdSe nanocrystals to ZnSe nanocrystals by sequential cation-exchange reactions proceeding via an intermediate $Cu_{2-x}Se$ nanocrystal composition. Whereas the first cation-exchange step (taking CdSe to $Cu_{2-x}Se$) proceeds rapidly at room temperature, the following step ($Cu_{2-x}Se$ to ZnSe) requires elevated temperatures (up to 250 °C), with trioctylphosphine added as a soft base to assist Cu^+ removal (and no added Se^{2-}). This transformation reaches completion within a few seconds at 250 °C.[21] Although less reactive than common Lewis acids used in cation exchange, Zn^{2+} has sufficient affinity for Se^{2-} for this reaction to proceed rapidly, and ripening is not problematic. In principle, a similar approach might possibly allow formation of $Cd_{1-x}Mn_xSe$ or related doped nanocrystals, but such chemistries have not yet been demonstrated.

Perhaps most closely related to the observations here is the synthesis of $Cd_{1-x}Zn_xSe$ alloy nanocrystals by heating core/shell CdSe/ZnSe nanocrystals.[58] In this chemistry, internal diffusion is believed to cause homogeneous alloying within minutes at temperatures above ∼290 °C. Ostwald ripening is evident at temperatures below this alloying point, but the size distribution can be kept relatively narrow ($\sigma \approx 5-12\%$). XRD data suggest a transformation from zinc blende to wurtzite may accompany this alloying.[58] A significant difference between this $Cd_{1-x}Zn_xSe$ nanocrystal synthesis and the present $Cd_{1-x}Mn_xSe$ nanocrystal synthesis is that MnSe is far less stable than ZnSe under the reaction conditions. Because of this instability, the $Cd_{1-x}Mn_xSe$ nanocrystals do not form via core/shell intermediates like the $Cd_{1-x}Zn_xSe$ nanocrystals do, longer times are needed to homogenize the $Cd_{1-x}Mn_xSe$ alloys (hours at 300 °C, Figure 3, compared to <5 min for the $Cd_{1-x}Zn_xSe$ alloys[58]), and $Cd_{1-x}Mn_xSe$ reaches smaller maximum values of x at equilibrium ($x_{Mn}(max) \approx 0.2$ vs $x_{Zn}(max) \approx 0.7$). The slower alloying in $Cd_{1-x}Mn_xSe$ nanocrystals in particular highlights the importance of suppressing Ostwald ripening, as achieved here. Despite these differences, these two processes may ultimately share a common mechanism. Notably, the $Cd_{1-x}Zn_xSe$ synthesis is also performed in the presence of excess cation and anion precursor, like in the present diffusion doping, and may therefore be assisted by the resulting high chemical potentials of these ions in solution. Given these similarities, it would be of interest to know whether CdSe/ZnSe alloying preserves nanocrystal shape anisotropies and whether conditions can be found under which crystallographic phases are also preserved. The results presented here for $Cd_{1-x}Mn_xSe$ nanocrystals suggest that both should be possible.

CONCLUSION

We have demonstrated a successful equilibrium synthesis of doped semiconductor nanocrystals. This method involves cation + anion addition to seed nanocrystals at elevated temperatures followed by diffusive mixing to yield the solid solution, akin to liquid−solid alloying of metals.[59] By suppressing Ostwald ripening, this method allows incorporation of relatively unreactive impurity ions while still retaining anisotropic shapes, size distributions, and crystallographic phases. This diffusion-doping method thus allows the nanocrystals to achieve their thermodynamic compositions without reaching their thermodynamically favored shapes, sizes, or crystallographic phases. Using this strategy, we have demonstrated the successful synthesis of high-quality colloidal $Cd_{1-x}Mn_xSe$ nanocrystals that simultaneously display the narrowest size distributions, the highest values of x, and the largest magneto-optical exciton splittings of any $Cd_{1-x}Mn_xSe$ nanocrystals reported to date. This success motivates the generalization of this strategy to synthesize nanocrystals of various other shapes and compositions under thermodynamic control, particularly compositions that do not involve the few well-known fast-diffusing ions that have dominated cation-exchange chemistries to date, and promising preliminary results for other nanocrystal compositions have been presented. Overall, these findings raise interesting possibilities for the development of new doped nanostructures with complex shapes and compositions, possibly including heterostructures, and may ultimately enable the advancement of new technologies involving this important class of materials.

ASSOCIATED CONTENT

Supporting Information

Additional synthetic details and experimental data. This material is available free of charge via the Internet at http://pubs.acs.org.

AUTHOR INFORMATION

Corresponding Author

gamelin@chem.washington.edu

Notes

The authors declare no competing financial interest.

ACKNOWLEDGMENTS

This work was supported by the U.S. National Science Foundation (NSF) (Grant DMR-1206221 to D.R.G.). Part of this work was conducted at the University of Washington NanoTech User Facility, a member of the NSF National Nanotechnology Infrastructure Network (NNIN). We thank Prof. Celso de Mello Donegá for fruitful discussions.

REFERENCES

(1) Murray, C. B.; Norris, D. J.; Bawendi, M. G. *J. Am. Chem. Soc.* **1993**, *115*, 8706.
(2) Alivisatos, A. P. *J. Phys. Chem.* **1996**, *100*, 13226.
(3) Murray, C. B.; Kagan, C. R.; Bawendi, M. G. *Annu. Rev. Mater. Sci.* **2000**, *30*, 545.
(4) Scholes, G. D. *Adv. Funct. Mater.* **2008**, *18*, 1157.
(5) de Mello Donegá, C. *Chem. Soc. Rev.* **2011**, *40*, 1512.
(6) Klimov, V. I. *Nanocrystal Quantum Dots*, 2nd ed.; CRC Press: Boca Raton, FL, 2010.
(7) Rogach, A. (Ed.) *Semiconductor Nanocrystal Quantum Dots. Synthesis, Assembly, Spectroscopy and Applications*. Springer: Vienna, Austria, 2008.
(8) Bryan, J. D.; Gamelin, D. R. *Prog. Inorg. Chem.* **2005**, *54*, 47.
(9) Erwin, S. C.; Zu, L. J.; Haftel, M. I.; Efros, A. L.; Kennedy, T. A.; Norris, D. J. *Nature* **2005**, *436*, 91.
(10) Norris, D. J.; Efros, A. L.; Erwin, S. C. *Science* **2008**, *319*, 1776.

(11) Beaulac, R.; Archer, P. I.; Ochsenbein, S. T.; Gamelin, D. R. *Adv. Funct. Mater.* **2008**, *18*, 3873.
(12) Beaulac, R.; Ochsenbein, S. T.; Gamelin, D. R. Colloidal Transition-Metal-Doped Quantum Dots. In *Nanocrystal Quantum Dots*, 2nd ed.; Klimov, V. I., Ed.; CRC Press: Boca Raton, FL, 2010; p 397.
(13) Buonsanti, R.; Milliron, D. J. *Chem. Mater.* **2013**, *25*, 1305.
(14) Sugimoto, T. *Adv. Colloid Interfac. Sci.* **1987**, *28*, 65.
(15) Furdyna, J. K.; Kossut, J. *Diluted Magnetic Semiconductors*; Academic: New York, 1988; Vol. *25* of Semicond. Semimet.
(16) Son, D. H.; Hughes, S. M.; Yin, Y.; Alivisatos, A. P. *Science* **2004**, *306*, 1009.
(17) Luther, J. M.; Zheng, H.; Sadtler, B.; Alivisatos, A. P. *J. Am. Chem. Soc.* **2009**, *131*, 16851.
(18) Jain, P. K.; Amirav, L.; Aloni, S.; Alivisatos, A. P. *J. Am. Chem. Soc.* **2010**, *132*, 9997.
(19) Casavola, M.; van Huis, M. A.; Bals, S.; Lambert, K.; Hens, Z.; Vanmaekelbergh, D. *Chem. Mater.* **2011**, *24*, 294.
(20) Miszta, K.; Dorfs, D.; Genovese, A.; Kim, M. R.; Manna, L. *ACS Nano* **2011**, *5*, 7176.
(21) Li, H.; Zanella, M.; Genovese, A.; Povia, M.; Falqui, A.; Giannini, C.; Manna, L. *Nano Lett.* **2011**, *11*, 4964.
(22) Rivest, J. B.; Jain, P. K. *Chem. Soc. Rev.* **2013**, *42*, 89.
(23) Mokari, T.; Aharoni, A.; Popov, I.; Banin, U. *Angew. Chem.* **2006**, *45*, 8001.
(24) Mocatta, D.; Cohen, G.; Schattner, J.; Millo, O.; Rabani, E.; Banin, U. *Science* **2011**, *332*, 77.
(25) Sahu, A.; Kang, M. S.; Kompch, A.; Notthoff, C.; Wills, A. W.; Deng, D.; Winterer, M.; Frisbie, C. D.; Norris, D. J. *Nano Lett.* **2012**, *12*, 2587.
(26) Acharya, S.; Sarkar, S.; Pradhan, N. *J. Phys. Chem. C* **2013**, *117*, 6006.
(27) Eilers, J.; Groeneveld, E.; de Mello Donega, C.; Meijerink, A. *J. Phys. Chem. Lett.* **2012**, *3*, 1663.
(28) Hagen, K. S.; Stephan, D. W.; Holm, R. H. *Inorg. Chem.* **1982**, *21*, 3928.
(29) Autissier, V.; Henderson, R. A. *Inorg. Chem.* **2008**, *47*, 6393.
(30) Chen, D.; Viswanatha, R.; Ong, G. L.; Xie, R.; Balasubramaninan, M.; Peng, X. *J. Am. Chem. Soc.* **2009**, *131*, 9333.
(31) Du, M.-H.; Erwin, S. C.; Efros, A. L. *Nano Lett.* **2008**, *8*, 2878.
(32) Erwin, S. C. *Phys. Rev. B* **2010**, *81*, 235433.
(33) Qu, L.; Peng, X. *J. Am. Chem. Soc.* **2002**, *124*, 2049.
(34) Carbone, L.; Nobile, C.; De Giorgi, M.; Della Sala, F.; Morello, G.; Pompa, P.; Hytch, M.; Snoeck, E.; Fiore, A.; Franchini, I. R.; Nadasan, M.; Silvestre, A. F.; Chiodo, L.; Kudera, S.; Cingolani, R.; Krahne, R.; Manna, L. *Nano Lett.* **2007**, *7*, 2942.
(35) Yu, W. W.; Qu, L.; Guo, W.; Peng, X. *Chem. Mater.* **2003**, *15*, 2854.
(36) Yu, W. W.; Peng, X. *Angew. Chem.* **2002**, *41*, 2368.
(37) Piepho, S. B.; Schatz, P. N. *Group Theory in Spectroscopy with Applications to Magnetic Circular Dichroism*; Wiley: New York, 1983.
(38) Beaulac, R.; Archer, P. I.; Liu, X.; Lee, S.; Salley, G. M.; Dobrowolska, M.; Furdyna, J. K.; Gamelin, D. R. *Nano Lett.* **2008**, *8*, 1197.
(39) Furdyna, J. K. *J. Appl. Phys.* **1988**, *64*, R29.
(40) Archer, P. I.; Santangelo, S. A.; Gamelin, D. R. *Nano Lett.* **2007**, *7*, 1037.
(41) Archer, P. I.; Santangelo, S. A.; Gamelin, D. R. *J. Am. Chem. Soc.* **2007**, *129*, 9808.
(42) Kuno, M.; Nirmal, M.; Bawendi, M. G.; Efros, A.; Rosen, M. *J. Chem. Phys.* **1998**, *108*, 4242.
(43) Shapira, Y.; Foner, S.; Ridgley, D. H.; Dwight, K.; Wold, A. *Phys. Rev. B* **1984**, *30*, 4021.
(44) Schwartz, D. A.; Norberg, N. S.; Nguyen, Q. P.; Parker, J. M.; Gamelin, D. R. *J. Am. Chem. Soc.* **2003**, *125*, 13205.
(45) Norberg, N. S.; Gamelin, D. R. *J. Appl. Phys.* **2006**, *99*, 08M104.
(46) Schimpf, A. M.; Gamelin, D. R. *J. Phys. Chem. Lett.* **2012**, *3*, 1264.
(47) Beaulac, R.; Gamelin, D. R. *Phys. Rev. B* **2010**, *82*, 224401.
(48) Beaulac, R.; Feng, Y.; May, J. W.; Badaeva, E.; Gamelin, D. R.; Li, X. *Phys. Rev. B* **2011**, *84*, 195324.
(49) Yu, W. W.; Qu, L.; Guo, W.; Peng, X. *Chem. Mater.* **2004**, *16*, 560 (erratum).
(50) Zhang, J.; Sun, K.; Kumbhar, A.; Fang, J. *J. Phys. Chem. C* **2008**, *112*, 5454.
(51) Bryan, J. D.; Schwartz, D. A.; Gamelin, D. R. *J. Nanosci. Nanotechnol.* **2005**, *5*, 1472.
(52) Beaulac, R.; Archer, P. I.; van Rijssel, J.; Meijerink, A.; Gamelin, D. R. *Nano Lett.* **2008**, *8*, 2949.
(53) Vlaskin, V. A.; Janssen, N.; van Rijssel, J.; Beaulac, R.; Gamelin, D. R. *Nano Lett.* **2010**, *10*, 3670.
(54) McLaurin, E. J.; Vlaskin, V. A.; Gamelin, D. R. *J. Am. Chem. Soc.* **2011**, *133*, 14978.
(55) McLaurin, E. J.; Fataftah, M. S.; Gamelin, D. R. *Chem. Commun.* **2013**, *49*, 39.
(56) Fedorov, V. A.; Ganshin, V. A.; Korkishko, Y. N. *Phys. Status Solidi A* **1993**, *139*, 9.
(57) Pradhan, N.; Peng, X. *J. Am. Chem. Soc.* **2007**, *129*, 3339.
(58) Zhong, X.; Han, M.; Dong, Z.; White, T. J.; Knoll, W. *J. Am. Chem. Soc.* **2003**, *125*, 8589.
(59) Larsson, L.-E. *Mater. Sci. Eng.* **1975**, *19*, 231.